BioMedical Engineering OnLine

RESEARCH

Open Access

Differentiation between invasive ductal carcinoma and ductal carcinoma in situ by combining intratumoral and peritumoral ultrasound radiomics

Heng Zhang[1,2,3,4], Tong Zhao[5], Jiangyi Ding[1,2,3,4], Ziyi Wang[1,2,3,4], Nannan Cao[1,2,3,4], Sai Zhang[1,2,3,4], Kai Xie[1,2,3,4], Jiawei Sun[1,2,3,4], Liugang Gao[1,2,3,4], Xiaoqin Li[5] and Xinye Ni[1,2,3,4*]

*Correspondence:
nxy@njmu.edu.cn

[1] Department of Radiotherapy Oncology, Changzhou No. 2 People's Hospital, Nanjing Medical University, Changzhou, China
[2] Jiangsu Province Engineering Research Center of Medical Physics, Changzhou, China
[3] Medical Physics Research Center, Nanjing Medical University, Changzhou, China
[4] Key Laboratory of Medical Physics in Changzhou, Changzhou, China
[5] Department of Ultrasound, Changzhou No.2 People's Hospital, Nanjing Medical University, Changzhou, China

Abstract

Background: This study aimed to develop and validate an ultrasound radiomics model for distinguishing invasive ductal carcinoma (IDC) from ductal carcinoma in situ (DCIS) by combining intratumoral and peritumoral features.

Methods: Retrospective analysis was performed on 454 patients from Chengzhong Hospital. The patients were randomly divided in accordance with a ratio of 8:2 into a training group (363 cases) and validation group (91 cases). In addition, 175 patients from Yanghu Hospital were used as the external test group. The peritumoral ranges were set to 2, 4, 6, 8, and 10 mm. Mann–Whitney *U*-test, recursive feature elimination, and a least absolute shrinkage and selection operator were used to in the dimension reduction of the radiomics features and clinical knowledge, and machine learning logistic regression classifiers were utilized to construct the diagnostic model. The area under the curve (AUC) of the receiver operating characteristics, accuracy, sensitivity, and specificity were used to evaluate the model performance.

Results: By combining peritumoral features of different ranges, the AUC of the radiomics model was improved in the validation and test groups. In the validation group, the maximum increase in AUC was 9.7% ($P=0.031$, AUC = 0.803) when the peritumoral range was 8 mm. Similarly, when the peritumoral range was only 8 mm in the test group, the maximum increase in AUC was 4.9% ($P=0.005$, AUC = 0.770). In this study, the best prediction performance was achieved when the peritumoral range was only 8 mm.

Conclusions: The ultrasound-based radiomics model that combined intratumoral and peritumoral features exhibits good ability to distinguish between IDC and DCIS. The selection of peritumoral range size exerts an important effect on the prediction performance of the radiomics model.

Keywords: Radiomics, Ultrasound, Breast cancer, Peritumoral features

Background

Breast cancer is a prevalent form of malignant tumor among women, with invasive ductal carcinoma (IDC) and ductal carcinoma in situ (DCIS) as the most frequently occurring types [1, 2]. Although both breast cancer types originate from cells of the breast duct, their treatment methods and expected outcomes differ [3]. IDC is a malignant tumor that is formed when cancer cells in the breast duct gradually spread to neighboring tissues. It usually has poor prognosis, and its 5-year survival rate is between 40 and 90%; it requires comprehensive treatment, including breast-conserving surgery, radiotherapy, and chemotherapy [4]. By contrast, DCIS is a superficial cancer, wherein cancer cells are confined to the breast duct and do not invade surrounding tissues or lymph nodes [5]. The prognosis for DCIS is generally good, with a 5-year survival rate higher than 90%, and radical surgical resection is the primary treatment method [6]. Research has indicated that about 10%–40% of cases diagnosed with DCIS through coarse needle puncture biopsy are confirmed as IDC via pathology after surgery, considerably affecting the choice of treatment plan and follow-up treatment of patients and causing patients to suffer from unnecessary pressure and panic [7, 8]. Therefore, accurately distinguishing between IDC and DCIS is of high significance before surgery. However, current diagnostic methods frequently require invasive procedures, such as surgery or puncture, which can lead to a long waiting time and complex processing with high uncertainty levels. A diagnostic method that is safer, faster, and more accurate should be developed urgently.

Radiomics is a noninvasive biomarker technology that utilizes image processing and machine learning to extract high-dimensional quantitative image features for describing tumors [9]. It can predict the prognosis of breast cancer patients by reflecting the heterogeneity of tumor cells and the microenvironment [10], providing important assistance to clinical decision-making. Recent studies have demonstrated that ultrasound radiomics can be an effective imaging biomarker, and it has been used in the early diagnosis of breast cancer [11, 12], molecular typing classification [13], efficacy evaluation [14, 15], and prognosis prediction [16, 17]. However, no study on distinguishing between IDC and DCIS on the basis of ultrasound radiomics has yet been conducted (PubMed, Web of Science). At present, most studies tend to solely focus on features within a tumor, disregarding the fact that features that surround a tumor also hold significant information. Tadayyon et al. [18] reported that quantitative ultrasound features combined with intratumoral and peritumoral features achieved better results in evaluating neoadjuvant chemotherapy response and predicting disease-free survival of breast cancer. Ocana et al. [19] believed that changes in peritumoral tissues are closely related to peritumoral lymphocyte infiltration. These findings indicate that considerable valuable information may be found in the peritumoral region. In addition, an increasing number of scholars are using peritumoral features in radiomics research. Yu et al. [20] extracted the features of the 2 mm peritumoral region from ultrasound images to improve the prediction effect of the disease-free survival of triple-negative breast cancer. Sun et al. [21] demonstrated that the radiomics features of intratumoral and peritumoral regions combined with tow-dimensional gray-scale ultrasound can better predict the status of the axillary lymph node metastasis of breast cancer. In their study, the peritumoral region was set as 5 mm. The aforementioned studies confirmed that the features around a tumor also provide valuable information in radiomics.

The purpose of the current study was to differentiate between IDC and DCIS by combining the features of intratumoral and peritumoral radiomics (shape, first-order, texture) as well as clinical knowledge and machine-learning logistic regression models. It further aimed to analyze the effectiveness of peritumoral features and the influence of peritumoral range size on the performance of the developed radiomics model.

Results

Baseline characteristics

A total of 629 patients from two hospitals were included in this study. Their detailed clinical and ultrasound characteristics are provided in Table 1. Patients with DCIS accounted for 21.9% (138/629) and patients with IDC accounted for 78.1% (491/629). In Chengzhong Hospital, patients with DCIS were younger than those with IDC ($P=0.006$), but this finding was not confirmed in Yanghu Hospital ($P=0.774$). In addition, no significant differences were found in tumor echo type, boundary, morphology, posterior features, orientation, and calcification between the DCIS and IDC groups in Chengzhong and Yanghu Hospitals (all $P>0.05$).

Table 1 Clinical and ultrasound characteristics

Group	Chengzhong Hospital ($n=454$)			Yanghu Hospital ($n=175$)		
	DCIS ($n=99$)	IDC ($n=355$)	*P* value	DCIS ($n=39$)	IDC ($n=136$)	*P* value
Age	49.0 (41.5,57.5)	53.0 (44.0,62.0)	0.009*	52 (48.5,59.5)	53.5 (47.75,63.25)	0.835
Echo type			0.628			0.591
Low	98 (99.0%)	353 (99.4%)		39 (100%)	135 (99.3%)	
Mix	1 (1.0%)	2 (0.6%)		0 (0%)	1 (0.7%)	
Boundary			0.249			0.290
Clear	2 (2.0%)	5 (1.4%)		0 (0%)	1 (0.7%)	
Blur	34 (34.3%)	90 (25.4%)		13 (33.3%)	47 (34.6%)	
Angulation	27 (27.3%)	91 (25.6%)		9 (23.1%)	32 (23.5%)	
Burr	11 (11.1%)	65 (18.3%)		11 (28.2%)	20 (14.7%)	
Differential blade	25 (25.3%)	104 (29.3%)		6 (15.4%)	36 (26.5%)	
Morphology			0.148			0.387
Circle	6 (6.1%)	9 (2.5%)		0 (0%)	4 (2.9%)	
Ellipse	14 (14.1%)	40 (11.3%)		5 (12.8%)	11 (8.1%)	
Irregularity	79 (79.8%)	306 (86.2%)		34 (87.2%)	121 (89.0%)	
Posterior feature			0.703			0.335
Echo enhancement	26 (26.3%)	106 (29.9%)		8 (20.5%)	39 (28.7%)	
Echo reduce	45 (45.4%)	146 (41.1%)		19 (48.7%)	49 (36.0%)	
No attenuation	28 (28.3%)	103 (29.0%)		12 (30.8%)	48 (35.3%)	
Orientation			0.411			0.071
Parallel	37 (37.4%)	149 (42.0%)		20 (51.3%)	48 (35.3%)	
Vertical	62 (62.6%)	206 (58.0%)		19 (48.7%)	88 (64.7%)	
Calcification			0.065			0.672
Positive	46 (46.5%)	202 (56.9%)		21 (53.8%)	68 (50.0%)	
Negative	53 (53.5%)	153 (43.1%)		18 (46.2%)	68 (50.0%)	

* Differences were significant at $P<0.05$

Feature selection

105 radiomics features were extracted from each intratumoral and peritumoral region, respectively, including 105 features from the intratumoral region, 68 features from peritumoral 2 mm, 84 features from peritumoral 4 mm, 93 features from peritumoral 6 mm, and 95 features from peritumoral 8 mm and 10 mm, exhibiting good intragroup/intergroup consistency (ICC > 0.75). Supplementary Fig. 1 provides the intratumoral and peritumoral radiomics feature ICC. Then, Mann–Whitney U-test, RFE, and Lasso were used to reduce the dimensions of the features, and a detailed feature screening process is illustrated in Supplementary Fig. 2. Finally, 9, 13, 16, 10, 12, and 10 features were included to construct the radiomics models of intratumoral, intratumoral + peritumoral 2 mm, intratumoral + peritumoral 4 mm, intratumoral + peritumoral 6 mm, intratumoral + peritumoral 8 mm, and intratumoral + peritumoral 10 mm, respectively. Interestingly, all the prediction models included several peritumoral features when combined with intratumoral peritumoral features. Separate peritumoral (2, 4, 6, 8, and 10 mm) radiomics models were composed of 4, 7, 2, 6, and 4 features, respectively. The detailed modeling feature information is presented in Supplementary Table 2.

Model development and validation

On the basis of the logistic regression model, 11 types of radiomics models for distinguishing between IDC and DCIS were established. They include intratumoral radiomics model, peritumoral (2, 4, 6, 8, and 10 mm) radiomics model, and intratumoral combined with peritumoral radiomics models (intratumoral + peritumoral 2 mm, intratumoral + peritumoral 4 mm, intratumoral + peritumoral 6 mm, intratumoral + peritumoral 8 mm, and intratumoral + peritumoral 10 mm). The ROC curves of these models in the training, validation, and test groups are shown in Fig. 1. Table 2 compares and analyzes the predictive performance of the intratumoral model and the peritumoral

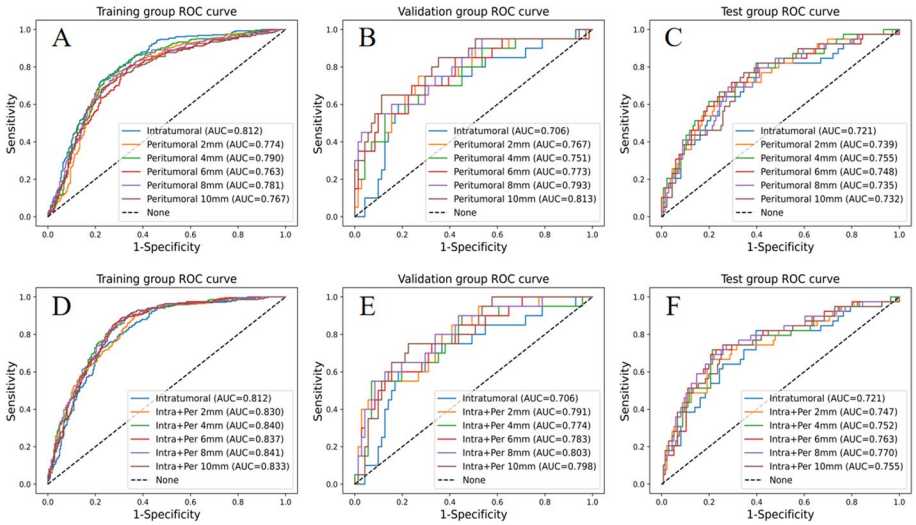

Fig. 1 ROC curves of the radiomics models for distinguishing between IDC and DCIS. Intra + Per, intratumoral combined with peritumoral. **A**–**C**, respectively, show the comparison of the AUCs of intratumoral and peritumoral radiomics models in the training, validation, and test groups. **D**–**F** respectively, show the comparison of the AUCs of intratumoral model and the combined intratumoral and peritumoral radiomics model in the training, validation, and test groups

Table 2 Comparison of the predictive performance of the intratumoral radiomics model and the peritumoral radiomics model with different peritumoral sizes

Model	AUC (95% CI)	Accuracy	Sensitivity	Specificity
Training group				
Intratumoral	0.812 (0.775–0.846)	0.745	0.761	0.729
Peritumoral 2 mm	0.774 (0.734–0.811)	0.734	0.757	0.711
Peritumoral 4 mm	0.790 (0.748–0.825)	0.743	0.754	0.732
Peritumoral 6 mm	0.763 (0.722–0.799)	0.718	0.761	0.676
Peritumoral 8 mm	0.781 (0.741–0.815)	0.731	0.761	0.701
Peritumoral 10 mm	0.767 (0.727–0.803)	0.725	0.743	0.708
Validation group				
Intratumoral	0.706 (0.568–0.823)	0.670	0.700	0.662
Peritumoral 2 mm	0.767 (0.631–0.878)	0.703	0.750	0.690
Peritumoral 4 mm	0.751 (0.614–0.870)	0.703	0.700	0.704
Peritumoral 6 mm	0.773 (0.641–0.888)	0.714	0.700	0.718
Peritumoral 8 mm	0.793 (0.663–0.908)	0.681	0.650	0.690
Peritumoral 10 mm	0.813 (0.690–0.923)	0.692	0.750	0.676
Test group				
Intratumoral	0.721 (0.625–0.819)	0.731	0.538	0.787
Peritumoral 2 mm	0.739 (0.641–0.832)	0.726	0.641	0.750
Peritumoral 4 mm	0.755 (0.657–0.843)	0.754	0.590	0.801
Peritumoral 6 mm	0.748 (0.646–0.836)	0.731	0.641	0.757
Peritumoral 8 mm	0.735 (0.633–0.825)	0.714	0.667	0.728
Peritumoral 10 mm	0.732 (0.635–0.819)	0.674	0.615	0.691

model. The results show that peritumoral features are equally useful in distinguishing between IDC and DCIS. Table 3 presents the changes in prediction performance of the model after combining peritumoral features of different ranges, particularly AUC (AUC is stable in unbalanced samples, while accuracy is easily affected by sample size). When combined with peritumoral features, the AUC of the models was improved to a certain extent, indicating the effectiveness of intratumoral features combined with peritumoral features in predicting IDC and DCIS. In the validation group, AUC was the highest when the peritumoral range was 8 mm. In the test group, AUC was also highest when the peritumoral range was 8 mm. This finding indicates that the performance of the radiomics model can be further improved by optimizing peritumoral range. In addition, the results demonstrated that in studies based on ultrasound intratumoral combined with peritumoral radiomics for predicting IDC and DCIS, the best results were obtained when peritumoral extent was 8 mm.

Comparison of models

The intratumoral combined with peritumoral radiomics model produced the highest AUC in the training, validation, and test groups compared with the intratumoral or peritumoral radiomics model only. In accordance with the DeLong test results in Table 4, a significant difference in AUC existed between the combined intratumoral and peritumoral models (except for 2 mm) and the intratumoral radiomics model in the training group (all $P<0.05$). In the validation group, significant differences in AUC were found between the combined intratumoral and peritumoral models and the intratumoral

Table 3 Comparison of the predictive performance of the intratumoral radiomics model and the intratumoral combined with peritumoral radiomics model with different peritumoral sizes

Model	AUC (95% CI)	Accuracy	Sensitivity	Specificity
Training group				
Intratumoral	0.812 (0.775–0.846)	0.745	0.761	0.729
Intra + Per 2 mm	0.830 (0.795–0.860)	0.739	0.750	0.729
Intra + Per 4 mm	0.840 (0.807–0.869)	0.776	0.803	0.750
Intra + Per 6 mm	0.837 (0.801–0.866)	0.769	0.789	0.750
Intra + Per 8 mm	0.841 (0.806–0.871)	0.771	0.799	0.743
Intra + Per 10 mm	0.833 (0.797–0.865)	0.768	0.792	0.743
Validation group				
Intratumoral	0.706 (0.568–0.823)	0.670	0.700	0.662
Intra + Per 2 mm	0.791 (0.679–0.892)	0.670	0.650	0.676
Intra + Per 4 mm	0.774 (0.646–0.889)	0.703	0.650	0.718
Intra + Per 6 mm	0.783 (0.667–0.887)	0.703	0.650	0.718
Intra + Per 8 mm	0.803 (0.682–0.904)	0.681	0.700	0.676
Intra + Per 10 mm	0.798 (0.695–0.893)	0.703	0.750	0.690
Test group				
Intratumoral	0.721 (0.625–0.819)	0.731	0.538	0.787
Intra + Per 2 mm	0.747 (0.642–0.838)	0.754	0.641	0.787
Intra + Per 4 mm	0.752 (0.654–0.842)	0.749	0.590	0.794
Intra + Per 6 mm	0.763 (0.670–0.855)	0.766	0.667	0.794
Intra + Per 8 mm	0.770 (0.674–0.862)	0.766	0.667	0.794
Intra + Per 10 mm	0.755 (0.659–0.850)	0.731	0.641	0.757

Intra + Per, intratumoral combined with peritumoral

Table 4 Comparisons of the AUC of the combined intratumoral and peritumoral radiomics model with their sub-radiomics models (intratumoral, peritumoral) in the training, validation, and test groups

Comparisons	Training group		Validation group		Test group	
	AUC		AUC		AUC	
	Z-score	*P* value	*Z*-score	*P* value	*Z*-score	*P* value
Intra + Per 2 mm vs intratumoral	1.878	0.060	2.233	0.026*	1.008	0.314
Intra + Per 2 mm vs peritumoral 2 mm	3.790	< 0.001*	0.492	0.623	0.246	0.806
Intra + Per 4 mm vs intratumoral	3.095	0.002*	2.047	0.041*	1.564	0.118
Intra + Per 4 mm vs peritumoral 4 mm	3.688	< 0.001*	0.474	0.636	− 0.096	0.924
Intra + Per 6 mm vs intratumoral	2.621	0.009*	3.029	0.002*	2.551	0.011*
Intra + Per 6 mm vs peritumoral 6 mm	5.079	< 0.001*	0.258	0.796	0.576	0.565
Intra + Per 8 mm vs intratumoral	3.112	0.002*	2.156	0.031*	2.814	0.005*
Intra + Per 8 mm vs peritumoral 8 mm	4.121	< 0.001*	0.180	0.857	1.305	0.192
Intra + Per 10 mm vs intratumoral	2.334	0.020*	1.983	0.047*	2.104	0.035*
Intra + Per 10 mm vs peritumoral 10 mm	4.010	< 0.001*	− 0.281	0.779	0.707	0.480

Intra + Per, intratumoral combined with peritumoral

* Differences were significant at $P < 0.05$

radiomics model (both $P < 0.05$). In the test group, only the combined intratumoral and peritumoral models at 6, 8, and 10 mm differed significantly from the intratumoral radiomics model in terms of AUC. For the AUC between the combined intratumoral and

peritumoral radiomics model and the peritumoral radiomics model, a significant difference was found between the training group (both $P < 0.05$), whereas no significant differences were noted between the validation and test groups (both $P > 0.05$).

Discussion

This work is the first systematic study on the effect of breast cancer ultrasound peritumoral range on the performance of a radiomics model. By comparing and analyzing the intratumoral, peritumoral, and combined radiomics models, we determined that the intratumoral, peritumoral, and combined ultrasound models can better distinguish between IDC and DCIS, and the combined peritumoral features can improve the performance of a model. This conclusion also confirms the results of some previous clinical and radiomics studies [18–21]: the peritumoral region and features contain additional information for quantitatively describing a tumor.

In this study, we generated peritumoral regions with different peritumoral ranges (2, 4, 6, 8, and 10 mm) and included the extracted peritumoral and intratumoral features in radiomics analysis. The results showed that when the peritumoral range was 8 mm, the AUC was the highest in the validation and test groups, i.e., 0.803 and 0.770, respectively. DeLong testing confirmed that significant differences existed between the AUC of this model and the intratumor radiomics model for the training, validation, and test groups. These results not only confirmed the importance of peritumoral features in radiomics studies, but also indicated that the selection of peritumoral range can affect the performance of radiomics models. Therefore, we suggest that systematic comparisons should be performed in peritumoral radiomics studies to determine the optimal peritumoral range (e.g., clinical breast cancer ultrasound generally determines the peritumoral range to be at 0–10 mm), rather than obtaining it arbitrarily or based on previous studies (many current studies have directly determined the peritumoral range to be at 4 mm), although such approach has been adopted in most current peritumoral radiomics studies. This strategy can further improve a prediction model and optimize its performance, providing a more accurate and reliable basis for the clinical application of radiomics.

With the development of high-frequency ultrasound technology in recent years, the detection rate of small lesions in the breasts has been significantly improved, making the diagnosis of DCIS with ultrasound possible [22]. In addition, predicting DCIS before surgery can effectively assist clinicians in optimizing the surgical plan, providing high clinical value. Moreover, in actual clinical application, the incidence of DCIS can reach as high as 20.0%–32.5% [23, 24]. This range of values is also consistent with our results (21.9%, 138/629). In accordance with the performance of the intratumoral radiomics model in the validation and test groups in Table 3, the ultrasound-based radiomics model can predict DCIS noninvasively before surgery. This condition is conducive to the development of personalized diagnosis and treatment plans. Previous clinical studies have shown that typical DCIS is characterized by slight hypoechoic mass, tiny lobulated edges, catheter dilation, no changes in the posterior echo, and enhanced blood flow signals in and around the lesion [25, 26]. Shi et al. [27] used ultrasound elastic imaging features to identify IDC and DCIS: they found that the velocity of lesion edge shear wave in IDC was significantly higher than that in DCIS. Moreover, the diagnostic AUC value was 0.66, initially confirming that ultrasound peritumoral features may help detect DCIS. Consistent with the aforementioned

results, our findings show that the intratumoral combined with the peritumoral radiomics model is more effective in predicting DCIS, with the highest AUC in the training, validation, and test groups. In addition, our ultrasound intratumoral combined with peritumoral radiomics model provides better prediction and is more stable than existing techniques for distinguishing between IDC and DCIS. Vy et al. [28] constructed a machine learning model for distinguishing between IDC and DCIS by using multi-clinical factors (clinical, X-ray, ultrasound imaging, and histopathological features). However, the performance of their model fluctuated considerably, with the accuracy rate fluctuating between 0.63 and 0.84. Li et al. [29] aimed to predict DCIS by using radiomics features from X-ray combined with clinical imaging features. The best AUC on the test group was 0.72, which was superior to that of the traditional clinical characterization method. However, the importance of peritumoral features was disregarded and prediction accuracy should be improved.

The current study has some limitations. First, it only considered the importance of peritumoral features for radiomics analysis in specific applications without conducting a detailed analysis of the effects of different clinical problems, image modes, scanning instruments, and imaging parameters. Second, the segmentation of image ROI via artificial segmentation may cause some deviations in the result. Therefore, the aforementioned problems should be verified individually in future studies. Moreover, the determination of the optimal peritumoral range should be combined with the analysis of specific clinical problems. The conclusion of this study is only applied to distinguishing between IDC and DCIS. In future studies, we need to further delve into the possible effects of different ultrasound probes and noise reduction techniques on the radiomics analysis. We plan to: (1) evaluate the differences in image quality and noise levels of different probes to understand their impact on the final radiomics diagnosis. (2) Explore the application of various noise reduction algorithms and assess their potential in improving image quality and accuracy of radiomics-based diagnosis. (3) To conduct a multi-center study to more fully evaluate the performance of different probes and the effectiveness of noise reduction strategies.

Conclusion

In summary, this study verified the feasibility of distinguishing IDC from DCIS by combining intratumoral with peritumoral ultrasound radiomics. It also revealed the importance of the peritumoral region in the radiomics analysis of breast cancer, demonstrating that peritumoral features can provide additional tumor information. In addition, this work is the first to systematically study the effect of peritumoral region size on the ultrasound radiomics analysis of breast cancer. The results showed that different peritumoral ranges can affect the performance of a radiomics model. Therefore, we suggest that the peritumoral range should be carefully optimized for specific clinical tasks and the most appropriate peritumoral range for modeling should be selected in future radiomics studies to improve clinical predictive performance.

Methods

Patients

This study was approved by our institutional review board and patient informed consent was waived. A retrospective analysis was performed on patients who received breast cancer treatment in two hospitals of our institution from January 2018 to February 2022.

The inclusion criteria were as follows: (1) patients receiving initial treatment for breast cancer in our hospital; (2) complete ultrasound images before treatment; and (3) a definite IDC or DCIS (pathological names in the medical record system). The exclusion criteria were as follows: (1) non-qualifying ultrasound images (damaged images or inability to identify the tumor site); (2) too long time between ultrasound examination and surgery or needle biopsy; (3) all or part of the clinical ultrasound features are missing; (4) history of preoperative treatments, such as neoadjuvant chemotherapy or radiotherapy; and (5) presence of multiple lesions. Finally, 629 patients were retained, including 454 patients from Chengzhong Hospital who were randomly divided into a training group and a validation group in accordance with a ratio of 8:2. Meanwhile, 175 patients from Yanghu Hospital were included in the external test group.

Ultrasound examinations and image interpretation

The ultrasonic diagnostic instruments used in this study were EPIQ5 and IU22 from Philips (the Netherlands), Esaote (Italy), Logio E9, Volusion E10 (GE) and Siemens s2000. A high-frequency linear array probe with frequency of 6–15 MHz was utilized in conjunction with the breast ultrasound mode. The patient was positioned supine, and her arms were raised to expose the breasts fully for examination. Scanning was performed on all quadrants of both breasts, with a focus on the lesion area.

The images were analyzed by two physicians with over 5 years and 10 years of experience in breast ultrasound. They utilized the US Breast Imaging Reporting and Data System [30] as reference. Any discrepancies between the diagnoses of the two physicians were resolved by a chief physician with 20 years of experience in breast ultrasound. The pathological findings remained unknown until physician image analysis had been performed. The six ultrasonic features evaluated for each mass were echo type (low or mix), boundary (clear, blur, angulation, burr, or differential blade), morphology (circle, ellipse, or irregularity), posterior features (echo enhancement, echo reduce, or no attenuation), orientation (parallel or vertical), and calcification (positive or negative).

Region of interest (ROI) segmentation and expansion

The original breast cancer images were imported into 3D Slicer software (V4.11), and ROIs were manually mapped along the tumor profiles by an experienced ultrasound physician (ultrasound physician 1, with more than 5 years of segmentation experience), who was blinded to the pathological results. Subsequently, 10 cases were randomly selected from IDC and DCIS in Chengzhong and Yanghu Hospitals, with a ratio of 1:1:1:1. These cases were assigned to another experienced ultrasound physician (ultrasound physician 2, with more than 10 years of segmentation experience) to assess the intergroup correlation coefficient (ICC) consistency of the radiomics features. After 1 week, ultrasound physician 1 re-outlined the ROIs of the same 40 images to evaluate intragroup correlation coefficient (ICC) consistency. A good consistency was indicated by ICC > 0.75. The formula for ICC is given in Eq. 1. Peritumoral expansion was performed using the following steps. First, an image was resampled to [1.0, 1.0] by using the SimpleITK (V2.1.1) package in Python 3.6 environment. Then, the ndimage image matrix processing function in the Scipy (V1.4.1) package was used to expand the ROI to 2, 4, 6, 8, and 10 mm

to obtain the peritumoral area. Figure 2 shows the representative original ultrasound images and intratumoral and peritumoral ROIs:

$$ICC = \frac{Cov(vc, vb)}{\sigma_{vc} \times \sigma_{vb}} \tag{1}$$

In Eq. (1), *vc* represents the extracted radiomics features data first mapped by ultrasound physician, *vb* represents the extracted radiomics features data second mapped by ultrasound physician 1 or first mapped by ultrasound physician 2, *Cov*(*vc*,*vb*) represents the covariance of *vc* and *vb*, σ_{vc} represents the standard deviation of *vc*, σ_{vb} represents the standard deviation of *vb*.

Radiomics feature extraction and preprocessing

We utilized Pyradiomics (V3.0.1, https://pyradiomics.readthedocs.io) [31], an open-source Python package, for image preprocessing and feature extraction in radiomics. The preprocessing steps involved the following. (1) Image normalization ensures the consistent scale and range of features, minimizing the effect of any variations in data factors or proportions on feature extraction. (2) In pre-clipping, the original image is clipped to the ROI size to reduce the calculation amount of feature extraction and exclude the influence of the tumor adjacent region. A total of 105 original features, which include shape, first-order, and texture features, were then extracted from the intratumoral and peritumoral ROIs of each patient. These features, which meet the Image Biomarker Standardization Initiative standard [32], are more interpretable and robust. Additional details of the radiomics features are provided in Supplementary Table 1 of the supplementary material.

Feature selection

To mitigate the effect of sample imbalance on model performance (IDC:DCIS = 491:138, samples tend to be classified into most categories), we oversampled the training group features (a combination of radiomics features and six ultrasonic features) by using the adaptive synthetic sampling method SMOTE [33] to achieve a 1:1 ratio. Then, we applied

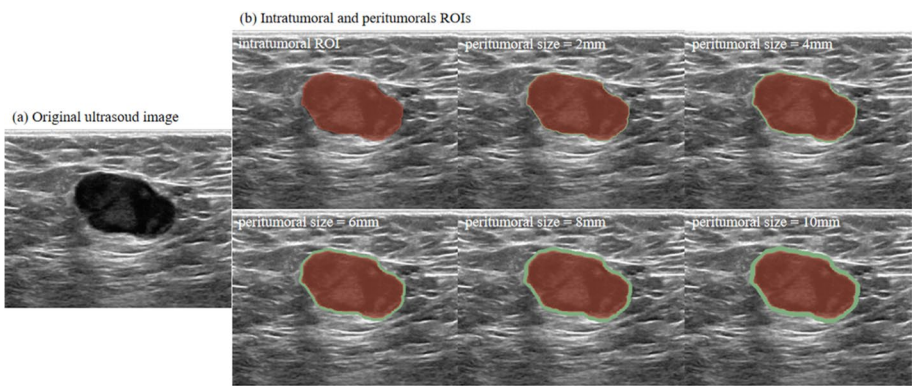

Fig. 2 Representative ultrasound images and their corresponding intratumoral and peritumoral ROIs. **a** Original ultrasound image. **b** Intratumoral ROI (red regions) and different ranges of peritumoral ROIs (green regions)

Z-score normalization to all the data to ensure the comparability of features by converting feature data with different orders of magnitude into the same order of magnitude. For select features, we employed a three-step screening method. First, on the basis of the Mann–Whitney U-test, features with statistical differences between patients with DCIS and IDC were screened out. Second, to avoid the overfitting phenomenon caused by too many features and meet the requirements of a lightweight clinical application, the recursive feature elimination (RFE) algorithm combined with random forest was used to iterate the remaining features one by one, and the top 10% features were retained. Finally, a least absolute shrinkage and selection operator (Lasso) for tenfold cross-validation was used for the final dimensional reduction. The dataset with the smallest cross-validation binomial deviation was chosen as the optimal feature subset for the construction of the diagnostic model.

Model development and validation

In the training group, we built radiomics models to distinguish between IDC and DCIS based on the final selection of features from radiomics features and clinical knowledge, (i.e., age, echo type, boundary, morphology, posterior feature, orientation, and calcification) and used a simple linear model (logistic regression). The performance of the models on the validation and test groups was evaluated more accurately by limiting the complexity of the models to reduce overfitting caused by excessive training data and by using a regularization method (i.e., the regularization operation L2 paradigm). Area under the receiver operating characteristics (ROC) curve (AUC), accuracy, sensitivity, and specificity were used as evaluation indicators, and the 95% confidence interval (CI) of AUC was obtained through 1000 resamples.

Statistical analysis

In this study, we used SPSS software for statistical analysis. For the categorization of data types, Age belongs to quantitative data, while Echo type, Boundary, Morphology, Posterior feature, Orientation and Calcification are qualitative data. We performed univariate analysis of these data separately to check whether they were significantly different in IDC and DCIS patients. Age data were quantitative and their distribution was first tested. If the age data conformed to a normal distribution, it was expressed as mean ± standard deviation ($x \pm s$) and differences between groups were compared using the independent samples *t*-test. If the age data did not conform to normal distribution, they were expressed as median (M) and quartiles (Q1, Q3) and compared using the independent samples Mann–Whitney U-test. For qualitative data, we used frequency counts and compared the differences between groups using the Chi-square test. The DeLong test was used to compare whether the difference between the AUC values of the combined intratumor combined with peritumor radiomics model was statistically significant compared to the intratumor or peritumor radiomics model alone in the training, validation, and test groups [34]. $P < 0.05$ was considered statistically significant.

Supplementary Information

The online version contains supplementary material available at https://doi.org/10.1186/s12938-024-01315-y.

Supplementary Material 1. Table 1. Overview of 105 Intratumoral radiomics features. Note: GLCM, gray-level cooccurrence matrix; GLRLM, gray-level run length matrix; GLSZM, gray level size zone matrix; GLDM, gray level dependence matrix; NGTDM, neighboring gray tone difference matrix. Table 2. Features included in different peritumoral range models. Intra+Per, intratumoral combined with peritumoral. Figure 1. ICC of various sizes in intratumoral and peritumoral radiomics models. Figure 2. Radiomics feature selection process. ICC, intra/inter–group correlation coefficient; M-W U-test, Mann–Whitney U-test; RFE, recursive feature elimination; LASSO, least absolute shrinkage, and selection operator; Intra+Per, intratumoral combined with peritumoral.

Author contributions

Conception and design: H.Z., T.Z., and X.N. Acquisition of data: H.Z., T.Z., and X.L. Analysis and interpretation of data: H.Z., T.Z., J. D., Z.W., N. C., S.Z., K.X., J. S., and L.G. Drafting or revising the article: H.Z., T.Z., K.X., J.S., L.G., and X. N. All authors have read and approved the manuscript.

Funding

This study was supported by the National Natural Science Foundation of China (No. 62371243), Jiangsu Provincial Medical Key Discipline Construction Unit (Oncology Therapeutics (Radiotherapy)) (No. JSDW202237), Social Development Project of Jiangsu Provincial Key Research & Development Plan (No. BE2022720), General Project of Jiangsu Provincial Health Commission (No. M2020006), Natural Science Foundation of Jiangsu Province (No. BK20231190) and Changzhou Social Development Project (No. CE20235063).

Availability of data and materials

No datasets were generated or analysed during the current study.

Declarations

Ethics approval and consent to participate

This retrospective study was approved by the Ethics Committee of the Affiliated Nanjing Medical University Changzhou Second People's Hospital (approval number: [2020]KY154-01) and the requirement for informed consent from all patients was waived.

Competing interests

The authors declare no competing interests.

Received: 16 July 2024 Accepted: 12 November 2024
Published online: 21 November 2024

References

1. Siegel RL, Miller KD, Wagle NS, Jemal A. Cancer statistics, 2023. CA Cancer J Clin. 2023;73(1):17–48.
2. Watkins EJ. Overview of breast cancer. JAAPA. 2019;32(10):13–7.
3. Esserman L, Yau C. Rethinking the standard for ductal carcinoma in situ treatment. JAMA Oncol. 2015;1(7):881–3.
4. Nigdelis MP, Karamouzis MV, Kontos M, Alexandrou A, Goulis DG, Lambrinoudaki I. Updates on the treatment of invasive breast cancer: Quo Vadimus? Maturitas. 2021;145:64–72.
5. van Seijen M, Lips EH, Thompson AM, Nik-Zainal S, Futreal A, Hwang ES, Verschuur E, Lane J, Jonkers J, Rea DW, et al. Ductal carcinoma in situ: to treat or not to treat, that is the question. Br J Cancer. 2019;121(4):285–92.
6. Hong YK, McMasters KM, Egger ME, Ajkay N. Ductal carcinoma in situ current trends, controversies, and review of literature. Am J Surg. 2018;216(5):998–1003.
7. Kim J, Han W, Lee JW, You JM, Shin HC, Ahn SK, Moon HG, Cho N, Moon WK, Park IA, et al. Factors associated with upstaging from ductal carcinoma in situ following core needle biopsy to invasive cancer in subsequent surgical excision. Breast. 2012;21(5):641–5.
8. Ding R, Xiao Y, Mo M, Zheng Y, Jiang YZ, Shao ZM. Breast cancer screening and early diagnosis in Chinese women. Cancer Biol Med. 2022;19(4):450–67.
9. Mayerhoefer ME, Materka A, Langs G, Häggström I, Szczypiński P, Gibbs P, Cook G. Introduction to radiomics. J Nucl Med. 2020;61(4):488–95.
10. Wang X, Xie T, Luo J, Zhou Z, Yu X, Guo X. Radiomics predicts the prognosis of patients with locally advanced breast cancer by reflecting the heterogeneity of tumor cells and the tumor microenvironment. Breast Cancer Res. 2022;24(1):20.
11. Luo WQ, Huang QX, Huang XW, Hu HT, Zeng FQ, Wang W. Predicting breast cancer in breast imaging reporting and data system (BI-RADS) ultrasound category 4 or 5 lesions: a nomogram combining radiomics and BI-RADS. Sci Rep. 2019;9(1):11921.
12. Xu Z, Wang Y, Chen M, Zhang Q. Multi-region radiomics for artificially intelligent diagnosis of breast cancer using multimodal ultrasound. Comput Biol Med. 2022;149: 105920.

13. Ferre R, Elst J, Senthilnathan S, Lagree A, Tabbarah S, Lu FI, Sadeghi-Naini A, Tran WT, Curpen B. Machine learning analysis of breast ultrasound to classify triple negative and HER2+ breast cancer subtypes. Breast Dis. 2023;42(1):59–66.
14. Jiang M, Li CL, Luo XM, Chuan ZR, Lv WZ, Li X, Cui XW, Dietrich CF. Ultrasound-based deep learning radiomics in the assessment of pathological complete response to neoadjuvant chemotherapy in locally advanced breast cancer. Eur J Cancer. 2021;147:95–105.
15. Yang M, Liu H, Dai Q, Yao L, Zhang S, Wang Z, Li J, Duan Q. Treatment response prediction using ultrasound-based pre-, post-early, and delta radiomics in neoadjuvant chemotherapy in breast cancer. Front Oncol. 2022;12: 748008.
16. Xiong L, Chen H, Tang X, Chen B, Jiang X, Liu L, Feng Y, Liu L, Li L. Ultrasound-based radiomics analysis for predicting disease-free survival of invasive breast cancer. Front Oncol. 2021;11: 621993.
17. Qiu X, Jiang Y, Zhao Q, Yan C, Huang M, Jiang T. Could ultrasound-based radiomics noninvasively predict axillary lymph node metastasis in breast cancer? J Ultrasound Med. 2020;39(10):1897–905.
18. Tadayyon H, Sannachi L, Gangeh MJ, Kim C, Ghandi S, Trudeau M, Pritchard K, Tran WT, Slodkowska E, Sadeghi-Naini A, et al. A priori prediction of neoadjuvant chemotherapy response and survival in breast cancer patients using quantitative ultrasound. Sci Rep. 2017;7:45733.
19. Ocaña A, Diez-Gónzález L, Adrover E, Fernández-Aramburo A, Pandiella A, Amir E. Tumor-infiltrating lymphocytes in breast cancer: ready for prime time? J Clin Oncol Oncol. 2015;33(11):1298–9.
20. Yu F, Hang J, Deng J, Yang B, Wang J, Ye X, Liu Y. Radiomics features on ultrasound imaging for the prediction of disease-free survival in triple negative breast cancer: a multi-institutional study. Br J Radiol. 2021;94(1126):20210188.
21. Sun Q, Lin X, Zhao Y, Li L, Yan K, Liang D, Sun D, Li ZC. Deep learning vs. radiomics for predicting axillary lymph node metastasis of breast cancer using ultrasound images: don't forget the peritumoral region. Front Oncol. 2020;10:53.
22. Moschetta M, Sardaro A, Nitti A, Telegrafo M, Maggialetti N, Scardapane A, Brunese MC, Lavelli V, Ferrari C. Ultrasound evaluation of ductal carcinoma in situ of the breast. J Ultrasound. 2022;25(1):41–5.
23. Knowlton CA, Jimenez RB, Moran MS. DCIS: risk assessment in the molecular era. Semin Radiat Oncol. 2022;32(3):189–97.
24. Virnig BA, Tuttle TM, Shamliyan T, Kane RL. Ductal carcinoma in situ of the breast: a systematic review of incidence, treatment, and outcomes. J Natl Cancer Inst. 2010;102(3):170–8.
25. Izumori A, Takebe K, Sato A. Ultrasound findings and histological features of ductal carcinoma in situ detected by ultrasound examination alone. Breast Cancer. 2010;17(2):136–41.
26. Li JK, Wang HF, He Y, Huang Y, Liu G, Wang ZL. Ultrasonographic features of ductal carcinoma in situ: analysis of 219 lesions. Gland Surg. 2020;9(6):1945–54.
27. Shi J, Chen L, Wang B, Zhang H, Xu L, Ye J, Liu Y, Shao Y, Sun X, Zou Y. Diagnostic value of ultrasound elastography in the differentiation of breast invasive ductal carcinoma and ductal carcinoma in situ. Curr Med Imaging. 2023;19(3):286–91.
28. Vy VPT, Yao MM, Le Khanh NQ, Chan WP. Machine learning algorithm for distinguishing ductal carcinoma in situ from invasive breast cancer. Cancers (Basel). 2022;14(10):2437.
29. Li J, Song Y, Xu S, Wang J, Huang H, Ma W, Jiang X, Wu Y, Cai H, Li L. Predicting underestimation of ductal carcinoma in situ: a comparison between radiomics and conventional approaches. Int J Comput Assist Radiol Surg. 2019;14(4):709–21.
30. Magny SJ, Shikhman R, Keppke AL. Breast imaging reporting and data system. Treasure Island (FL): StatPearls Publishing LLC; 2021.
31. van Griethuysen JJM, Fedorov A, Parmar C, Hosny A, Aucoin N, Narayan V, Beets-Tan RGH, Fillion-Robin JC, Pieper S, Aerts HJWL. Computational radiomics system to decode the radiographic phenotype. Cancer Res. 2017;77(21):e104–7.
32. Zwanenburg A, Vallières M, Abdalah MA, Aerts HJWL, Andrearczyk V, Apte A, Ashrafinia S, Bakas S, Beukinga RJ, Boellaard R, et al. The image biomarker standardization initiative: standardized quantitative radiomics for high-throughput image-based phenotyping. Radiology. 2020;295(2):328–38.
33. Chawla NV, Bowyer KW, Hall LO, Kegelmeyer WP. SMOTE: synthetic minority over- sampling technique. J Artif Intell Res. 2002;16:321–57.
34. DeLong ER, DeLong DM, Clarke-Pearson DL. Comparing the areas under two or more correlated receiver operating characteristic curves: a nonparametric approach. Biometrics. 1988;44(3):837–45.

Publisher's Note